JOURNAL OF GUIDANCE, CONTROL, AND DYNAMICS
Vol. 27, No. 1, January–February 2004

Frenet-Based Algorithm for Trajectory Prediction

Giulio Avanzini*
Politecnico di Torino, 10129 Turin, Italy

An algorithm for aircraft trajectory prediction is presented that is based on two algebraic representations of the aircraft c.g. trajectory in the Frenet frame: (1) a cylindrical helix, during steady flight segments, and (2) a third-order accurate expansion, during transient maneuvering phases. This technique allows for an efficient evaluation of future c.g. positions in a time interval the extension of which depends on the aircraft maneuver state, without requiring the implementation of the aircraft dynamic model. A Kalman filtering technique with a fixed-lag smoother is used for simultaneously filtering the sensor noise and estimating accelerometer and rate-gyro signal derivatives. The effect of a step variation of commanded load factor and/or roll angle on the aircraft position at following times is displayed to the pilot as a visual aid for representing achievable future positions during the maneuver. The algorithm is demonstrated by computer simulation of reverse turn maneuvers of an F-16 fighter aircraft model.

Nomenclature

$\boldsymbol{A}$	=	agility vector (time derivative of the acceleration); state matrix of the continuous-time Markov process
$\boldsymbol{a}$	=	acceleration vector
$\boldsymbol{a}_{\text{acc}}$	=	accelerometer output, $(a_{\text{acc},x}, a_{\text{acc},y}, a_{\text{acc},z})^T$
$a_{i,j}$	=	element of $\boldsymbol{A}$
$\boldsymbol{a}_n$	=	normal component of the acceleration
$\boldsymbol{B}$	=	input matrix of the continuous-time Markov process
$\boldsymbol{b}$	=	binormal unit vector
$\boldsymbol{C}$	=	output matrix
$\boldsymbol{D}$	=	Kalman filter dynamic matrix
$\boldsymbol{g}$	=	gravity acceleration vector
h	=	altitude
$\boldsymbol{I}$	=	identity matrix
$\boldsymbol{K}$	=	steady-state Kalman filter gain matrix
K_{ARI}	=	aileron–rudder interconnect gain
K_W	=	weight coefficient
k	=	discrete time
k_1, k_2	=	intrinsic variables (curvature and torsion)
L	=	Kalman smoother lag
$\boldsymbol{L}_{BI}, \boldsymbol{L}_{BF}, \boldsymbol{L}_{FI}$	=	rotation matrices
m	=	number of estimated time derivatives of the signal $x(t)$
$\boldsymbol{n}$	=	normal unit vector
n_z	=	normal load factor
$\boldsymbol{Q}$	=	covariance matrix of the discrete-time system
$q_{i,j}$	=	element of $\boldsymbol{Q}$
$\boldsymbol{R}$	=	position vector of c.g. in the inertial frame
$\boldsymbol{R}_A$	=	position of the accelerometers in body frame, $(x_A, y_A, z_A)^T$
r	=	autocorrelation function of the innovation process
s	=	curvilinear abscissa
T	=	sampling time
t	=	time
$\boldsymbol{t}$	=	tangent unit vector
V	=	velocity modulus
$\boldsymbol{V}$	=	velocity vector
v	=	observation (Gaussian white) noise
$\boldsymbol{W}$	=	process (Gaussian white) noise of the discrete-time system
w	=	process (Gaussian white) noise
$\boldsymbol{X}$	=	discrete-time state vector, $\boldsymbol{x}(kT)$
x	=	estimated variable
$\boldsymbol{x}$	=	continuous-time state vector, $(x, \mathrm{d}x/\mathrm{d}t, \mathrm{d}^2x/\mathrm{d}t^2, \ldots, \mathrm{d}^m x/\mathrm{d}t^m)^T$
$(x_F, y_F, z_F)^T$	=	position vector in the Frenet frame
y	=	noise corrupted measure of x
α	=	angle of attack
δ_A, δ_R	=	aileron and rudder deflection
$\lambda_{\max}$	=	dominant eigenvalue of $\boldsymbol{D}$
ρ	=	radius of the helix
σ_v^2	=	measurement noise variance of the continuous-time Markov process
σ_w^2	=	process noise variance of the continuous-time Markov process
$\boldsymbol{\Phi}$	=	state matrix of the discrete-time system
ϕ	=	roll angle
$\boldsymbol{\omega}$	=	angular velocity, $(p, q, r)^T$

Subscripts

A	=	in the accelerometer position
acc	=	accelerometers
B	=	body frame
est	=	estimated
F	=	Frenet frame
G	=	in the c.g.
I	=	inertial frame

Superscripts

$\hat{}$	=	Kalman filter estimate
$*$	=	augmented

I. Introduction

THE problem of trajectory prediction is encountered whenever it is necessary to provide the pilot or the control system with a projection of the future position of the aircraft, given the current flight condition, together with an envelope of feasible trajectories. This can be particularly useful during accurate flight-path tracking phases, such as in-flight refueling, for military jets, or prescribed landing steep approaches, for modern civil transport aircraft with

Presented as Paper 2000-3997 at the AIAA Atmospheric Flight Mechanics Conference, Denver, CO, 14–17 August 2000; received 1 October 2002; revision received 20 June 2003; accepted for publication 25 June 2003.

*Assistant Professor, Department of Aeronautical and Space Engineering, C.so Duca degli Abruzzi 24. Member AIAA.

short takeoff and landing capabilities. In the latter case, the predicted trajectory can be shown to the pilot by the head-up display (HUD) to compare current, future, and desired location. In recent works, Grunwald[1,2] and Sachs[3] demonstrated a significant improvement in terms of pilot rating, preciseness of control, and control activity when a three-dimensional perspective display of the commanded flight path (the so-called tunnel in the sky virtual display) is aided by a predictive information on the future aircraft location.

Trajectory prediction is also crucial in nap-of-the-Earth flight of highly automated rotorcraft or unmanned and autonomous aerial vehicles.[4] The prediction can be integrated in a ground proximity warning system, to reveal a possible ground collision with a time margin sufficient for undertaking an appropriate control action for avoiding obstacles on the prescribed flight path. In this case, the knowledge of an envelope of feasible future positions is also useful, if an efficient guidance law for obstacle avoidance is sought. The same approach could also be used for civil transport in critical flight regimes, such as one-engine-out takeoff maneuvers.

In a more complex framework, it is also possible to combine the trajectory prediction algorithm with a predictive control system.[5,6] In this case, the control action is determined to match the future predicted plant output with the prescribed one, inside a given prediction horizon, the extension of which depends on the plant dynamics. In most of the reported applications of predictive algorithmic control, a linear plant is considered as, for instance, the terrain-following scheme proposed by Reid et al.[7] or the tracking algorithm of Jung and Hess.[8]

In this paper, an accurate and efficient algorithm for determining future positions of the aircraft c.g. inside a given prediction horizon from measurements of acceleration and angular velocity is presented. The technique is based on the weighted combination of two estimates: (1) the projection in the Frenet frame of a helix with vertical axis (see Ref. 9), for long-term prediction in steady and quasi-steady maneuvering segments, and (2) a third-order accurate power series expansion of the trajectory in the Frenet frame (see Ref. 9), useful for short-term trajectory prediction during transient maneuvering phases. The first case includes, as degenerate cases, steady rectilinear trajectories and level turns.

The coefficients of both the estimates depend on the trajectory intrinsic coordinates, curvature and torsion. The intrinsic variables and the Frenet frame can be determined as a function of aircraft velocity, acceleration, and agility vector (see Refs. 9 and 10) and are, thus, made available from measurement of elementary kinematic quantities. The possibility of describing aircraft trajectories by means of these geometric quantities was recognized by Miele,[11] but to the author's knowledge, this is the first application of such a description in the framework of aircraft trajectory prediction.

The technique is computationally efficient, as far as only algebraic relations between aircraft acceleration, angular velocity, and their time derivatives are involved in the estimate of the position vector increment. Moreover, the estimation of wind velocity components is not required because the prediction is based on measurement of inertial quantities, regardless of the actual aircraft dynamics. This fact represents a considerable advantage over other techniques, where future output estimates are obtained from a model of the plant, as in classical predictive control algorithms.[5–8] In this case, a knowledge (or an estimate) of both low- and high-frequency disturbances is necessary because, when trajectory prediction of an aircraft is dealt with, a nonzero mean wind velocity can introduce large errors in long-term predictions, whereas atmospheric turbulence can have an influence on the aerodynamic force and moments. Thus, relatively large errors are introduced in short-term predictions. In the present approach, long-term prediction during steady flight phases would be only marginally spoilt by the presence of a nonzero mean wind, whereas the effect of turbulence on short-term prediction is practically negligible, inasmuch as variations of linear and angular velocity and acceleration are immediately taken into consideration as soon as they have an impact on the aircraft flight condition.

Note that also the circular flight-path continuation technique, adopted in Refs. 1–3, is based on a prediction determined from measured quantities only. In Refs. 1–3, the importance of the predictor performance in virtual visual aids to the pilot for compensatory flight-path control is greatly emphasized (as for the cited tunnel in the sky) to improve the situation awareness and to reduce the control action. These works deserve a more detailed analysis.

In both planar and longitudinal maneuvers, the predictor is based on a circular flight-path, the radius of which is evaluated from the current values of the trajectory variables: heading angle and turn rate, in the first case[1,2] and climb angle and its time derivative in the second one.[3] The basic predictor generates an estimate of the position error with respect to the commanded flight path at the prediction time T_p on the basis of a second-order approximation of the osculating circle. The prediction time is chosen on the basis of control consideration, to obtain the best equalization of the loop closure by the pilot of the predictor-aircraft element.[1,3]

Corrections to the basic predictor are introduced in the planar case to compensate for some of the major problems encountered, such as corner cutting in transition phases (from straight to turning flight and vice versa) and loss of accuracy in presence of low-frequency disturbances and biases. In the case of the longitudinal maneuver, a correction of the gains of the predictor system is introduced to obtain a type 1 response in the crossover frequency range of the pilot-system.[3]

It is the author's opinion that the circular flight path is not suitable for dealing with tridimensional trajectories, even in the simple case of a steady climbing turn. The reasons are that 1) the coupling between longitudinal and lateral–directional dynamics in turning flight cannot be taken into consideration in any way, unless a very complex scheduling of the gains is introduced as a function of airspeed, turn rate, and climb angle, and 2) the longitudinal and lateral–directional characteristics of the aircraft may cause the prediction horizon of the longitudinal and planar predictors to differ significantly, so that it seems very difficult to merge properly the two predictions into a single forecast in a three-dimensional space. Moreover, the choice of different values for T_p in the proportional and integral gains of the longitudinal predictor makes the algorithm unsuitable for application in obstacle avoidance and ground proximity warning systems because the physical meaning of the predictor output as forecast of the future position is lost. Finally, the choice of T_p and of most of the correction factors is based on the knowledge of the dynamic characteristics of the aircraft, with consequent loss of generality, inasmuch as tailoring of the algorithm is necessary when changing type of aircraft, extensive pilot testing being strongly recommended to achieve satisfactory performance.

The accuracy of the trajectory expansion in the Frenet frame was thoroughly discussed in Refs. 9 and 12, where both direct[9] and inverse[12] simulation algorithms based on the principle of timescale separation were presented. In those cases, the expansion in the Frenet frame was used to solve the slow-timescale trajectory problem on the basis of simple algebraic relations. The timescale separation principle also plays a major role in the present trajectory prediction algorithm because the variation of the trajectory variables following pilot inputs or external disturbances is slow, if compared to attitude variables. This fact allows for the determination of future positions on the basis of current values of trajectory curvature and torsion for a finite time step.

In steady-state flight, any trajectory can be represented in terms of a (possibly degenerate) cylindrical helix, torsion being zero for steady level turns and motions in the longitudinal plane, whereas both curvature and torsion are zero for rectilinear flight segments. Thus, as a first advantage, the algorithm needs not to be rephrased when dealing with planar or longitudinal maneuvers. Moreover, the use of curvature and torsion allows for an accurate position prediction with an arbitrary prediction horizon for any steady flight condition. When the maneuver state is changed by the pilot, a short-term prediction is still possible using the third-order accurate expansion of the trajectory in the Frenet frame.

A peculiar aspect of the present prediction algorithm is that estimation of time derivatives of acceleration and angular velocity vector components is required because, when the accelerometers are not located at the aircraft c.g., as it is usually the case, the body-frame components of the time derivative of the acceleration depend

on the derivative of the accelerometer signals and the first and second derivatives of the rate-gyro output.

Derivative estimation from noisy signals is not a trivial task, and a Kalman filter is adopted to obtained smoothed estimates of both the sensor signals and their derivatives. The filter is based on a revised version of the off-line smoother proposed by Fioretti and Jetto in Ref. 13, applied in an aircraft parameter identification framework by Hoff and Cook.[14] In both Refs. 13 and 14, off-line signal filtering and derivative estimation are dealt with, so that a fixed-lag Kalman smoother was used with no restriction on the computational effort and time delay necessary for obtaining the smoothed estimate of the signal and of its derivatives. In the present case, a real-time implementation of the filter is sought, and for this reason, on-line smoother performance is to be accurately evaluated, inasmuch as the delay introduced by the smoothing process must be kept as low as possible, as will be thoroughly discussed in Sec. II.

As a further application of the trajectory approximation, the prediction of a cone of feasible future positions is determined, to evaluate the influence of pitch and roll commands on the future flight path. The introduction of aircraft performance limits, such as the maximum admissible load factor, in the evaluation of the feasible set of future locations is straightforward. A perspective view of the envelope of feasible positions at different times as a function of pitch and roll commands can, thus, be projected on the HUD in the same way as for the commanded trajectory tunnel of Refs. 1–3. In this way, the information displayed to the pilot on the HUD on the future position of the aircraft is completed by the set of future locations that can be reached by a proper control action.

In what follows, the proposed method for predicting future aircraft c.g. positions is presented. The technique for evaluating the coefficients of the expansion from noise-corrupted signals coming from accelerometers and rate gyros is also briefly discussed. Then, the accuracy of the algorithm in predicting the future aircraft location is evaluated for three turn-reversal maneuvers of an F-16 fighter aircraft model. A section of conclusions ends the paper.

II. Analysis

Aircraft Trajectory in the Frenet Frame

Given a curve $\boldsymbol{R}(t)$ in a three-dimensional space (an aircraft trajectory, in the present application), the Frenet frame is defined, for each point of the curve, by the following unit vectors:

Tangent unit vector:

$$\boldsymbol{t} = \boldsymbol{V}/V \tag{1a}$$

Normal unit vector:

$$\boldsymbol{n} = \boldsymbol{a}_n/\|\boldsymbol{a}_n\| \tag{1b}$$

Binormal unit vector:

$$\boldsymbol{b} = \boldsymbol{t} \times \boldsymbol{n} \tag{1c}$$

where $\boldsymbol{a}_n = \boldsymbol{a} - \dot{V}\boldsymbol{t}$ is the normal component of the acceleration vector $\boldsymbol{a}$ in the osculating plane and $\times$ is the symbol for the vector cross product. For any point P, it is also possible to define the so-called intrinsic variables k_1 and k_2, curvature (or first curvature) and torsion (or second curvature), respectively, expressed as

$$k_1 = (1/V^2)\sqrt{\boldsymbol{a}\cdot\boldsymbol{a} - (\boldsymbol{a}\cdot\boldsymbol{t})^2}$$

$$k_2 = \det(\boldsymbol{V}\vdots\boldsymbol{a}\vdots\boldsymbol{A})/\{V^2[\boldsymbol{a}\cdot\boldsymbol{a} - (\boldsymbol{a}\cdot\boldsymbol{t})^2]\} \tag{2}$$

where $\boldsymbol{A}$ is the agility vector, defined as the time derivative of the acceleration.[15]

Under the hypothesis of motion over a flat, nonrotating Earth and neglecting variations of air density with altitude, a steady turn condition results into a trajectory represented by a cylindrical helix with vertical axis, that is, a climbing or gliding turn.[16] Curvature and torsion are constant along a cylindrical helix, so that these two parameters are sufficient for determining future positions along any steady flight path, with an arbitrary prediction horizon, in the absence of external disturbances. If the climb angle is zero (as for a level turn), the advance ratio of the helix becomes zero, and the helix degenerates into a circle, with $k_2 = 0$; whereas if the radius of curvature is infinite, the helix degenerates into a straight flight path, with $k_1 = 0$ and $k_2 = 0$.

Choosing the aircraft c.g. location at $t = t_0$ as the origin of the inertial reference frame, with the x axis oriented along the projection of the aircraft velocity in the horizontal plane and the z axis along the vertical direction, the aircraft trajectory in a steady turn can be expressed as

$$\boldsymbol{R}(t) = \begin{pmatrix} \rho\sin[\omega(t-t_0)] \\ \rho\{1-\cos[\omega(t-t_0)]\} \\ -\dot{h}(t-t_0) \end{pmatrix} \tag{3}$$

where $\omega = \|\boldsymbol{\omega}\|$ is the modulus of the angular velocity, $\dot{h}$ is the climb rate, and the radius ρ of the helix satisfies the relation

$$V^2 = (\omega\rho)^2 + \dot{h}^2$$

With use of Eqs. (2), the (constant) values of curvature and torsion along a steady-state trajectory are given by

$$k_1 = (1/\rho)[1-(\dot{h}/V)^2], \qquad k_2 = -\dot{h}\sqrt{V^2-\dot{h}^2}\big/(\rho V^2) \tag{4}$$

With use of definitions (1), the rotation matrix $\boldsymbol{L}_{FI}$ can be obtained, to represent the components of $\boldsymbol{R}(t)$ in the Frenet frame. From Eqs. (1), (3), and (4), after some tedious algebra, the trajectory of the aircraft in the Frenet frame is expressed as

$$\begin{pmatrix} x_F \\ y_F \\ z_F \end{pmatrix} = \begin{pmatrix} \dfrac{k_2^2}{k_1^2+k_2^2}s + \dfrac{k_1^2}{\left(k_1^2+k_2^2\right)^{\frac{3}{2}}}\sin\left(s\sqrt{k_1^2+k_2^2}\right) \\ \dfrac{k_1}{k_1^2+k_2^2}\left[1-\cos\left(s\sqrt{k_1^2+k_2^2}\right)\right] \\ \dfrac{k_1k_2}{k_1^2+k_2^2}s - \dfrac{k_1k_2}{\left(k_1^2+k_2^2\right)^{\frac{3}{2}}}\sin\left(s\sqrt{k_1^2+k_2^2}\right) \end{pmatrix} \tag{5}$$

where the curvilinear abscissa, s, for a steady flight condition, is given by $s = V(t-t_0)$.

For an arbitrary trajectory, a third-order accurate expansion in the Frenet frame from a point P on the flightpath is given by[9]

$$\begin{pmatrix} x_F \\ y_F \\ z_F \end{pmatrix} = \begin{pmatrix} s - \dfrac{1}{3!}(k_1)_P^2 s^3 \\ \dfrac{1}{2!}(k_1)_P s^2 + \dfrac{1}{3!}\left(\dfrac{\partial k_1}{\partial s}\right)_P s^3 \\ \dfrac{1}{3!}(k_1k_2)_P s^3 \end{pmatrix} \tag{6}$$

Equation (6) can be used for short-term predictions during nonsteady flight maneuvers. The prediction horizon, in this case, depends on the maneuver itself and is shorter for aggressive maneuvering, but nonetheless more accurate than a simple prediction based on a circular flight-path continuation.

The transformation matrix from the Frenet to the body frame $\boldsymbol{L}_{BF} = (\boldsymbol{t}\vdots\boldsymbol{n}\vdots\boldsymbol{b})$ is used for projecting the position increment $\Delta\boldsymbol{R}_F = (x_F, y_F, z_F)^T$ from the local Frenet frame at present time t_0 into the body frame. In particular, $\Delta\boldsymbol{R}_B = \boldsymbol{L}_{BF}\Delta\boldsymbol{R}_F$ can be interpreted as the position prediction as seen by the pilot. When a_n is zero, as in steady rectilinear flight, the trajectory curvature vanishes, while the normal and binormal unit vectors and the torsion become undefined. For this reason, when a_n gets close to zero, a simple prediction along a rectilinear path describes the aircraft motion. The rotation matrix used is $\tilde{\boldsymbol{L}}_{BF} = (\boldsymbol{t}\vdots\tilde{\boldsymbol{n}}\vdots\tilde{\boldsymbol{b}})$, where $\tilde{\boldsymbol{n}}$ is the unit vector perpendicular to $\boldsymbol{t}$, that lies in the vertical plane, directed downward, and, again, it is $\tilde{\boldsymbol{b}} = \boldsymbol{t}\times\tilde{\boldsymbol{n}}$.

Given the current position $\boldsymbol{R}(t_0)$, it is also possible to estimate the future inertial position $\boldsymbol{R}_{\text{est}}(t)$, with a further projection of $\Delta\boldsymbol{R}_B$ from the body to the inertial frame

$$\boldsymbol{R}_{\text{est}}(t) = \boldsymbol{R}(t_0) + \boldsymbol{L}_{IB}(t_0)\boldsymbol{L}_{BF}(t_0)\Delta\boldsymbol{R}_F[s(t-t_0)] \tag{7}$$

According to Eq. (1), the determination of the matrix $\boldsymbol{L}_{BF}$ requires the measurement of the components of velocity and acceleration in the body frame.

As far as the intrinsic coordinates depend on kinematic quantities only, the focus of the paper lies on the capability of estimating the coefficients in Eq. (2) from noisy acceleration and angular rate measurements, and it will be assumed that aircraft velocity and attitude angles are made available to the algorithm by some external source, such as an inertial measuring unit (IMU) with integrated global positioning system (GPS) receiver.

Evaluation of Acceleration and Agility Vector Components

The accelerometer output is nominally proportional to the difference between inertial and gravity acceleration,[17]

$$\boldsymbol{a}_{\text{acc}} = \boldsymbol{a}_A - \boldsymbol{L}_{BI}\boldsymbol{g} \tag{8}$$

where A is the accelerometer location, determined in the body frame by the vector $\boldsymbol{R}_A = (x_A, y_A, z_A)^T$ with respect to the aircraft c.g. position. Accordingly, the c.g. acceleration is given as a function of the accelerometer output by

$$\boldsymbol{a}_G = \boldsymbol{a}_{\text{acc}} + \boldsymbol{L}_{BI}\boldsymbol{g} - \dot{\boldsymbol{\omega}} \times \boldsymbol{R}_A - \boldsymbol{\omega} \times \boldsymbol{\omega} \times \boldsymbol{R}_A \tag{9}$$

To determine the curvature k_1, only c.g. velocity and acceleration components are required, and the agility vector in Eq. (2) is given by

$$\boldsymbol{A}_G = \dot{\boldsymbol{a}}_G + \boldsymbol{\omega} \times \boldsymbol{a}_G \tag{10}$$

With use of Eq. (9), it is

$$\dot{\boldsymbol{a}}_G = \dot{\boldsymbol{a}}_{\text{acc}} - \boldsymbol{\omega} \times \boldsymbol{L}_{BI}\boldsymbol{g} - \ddot{\boldsymbol{\omega}} \times \boldsymbol{R}_A - \dot{\boldsymbol{\omega}} \times \boldsymbol{\omega} \times \boldsymbol{R}_A - \boldsymbol{\omega} \times \dot{\boldsymbol{\omega}} \times \boldsymbol{R}_A \tag{11}$$

Therefore, both the expansions (5) and (6) of the c.g. trajectory in the Frenet frame require the evaluation of $\dot{\boldsymbol{a}}_G$, $\dot{\boldsymbol{\omega}}$, and $\ddot{\boldsymbol{\omega}}$.

Estimation of Derivatives of Noisy Signals

The technique proposed by Fioretti and Jetto[13] appears suitable for sensor signal differentiation, inasmuch as smoothed values of the signal and an estimate of its derivatives up to a given order m are simultaneously provided. Unfortunately, the online implementation is not straightforward because the filter gains can be evaluated only once the whole signal is acquired and the smoother introduces a sizable delay in the evaluation of the estimates. In the sequel, together with a brief presentation of the principal features of the method, a detailed description of which is reported in Ref. 13, the technique devised for the present online implementation of the algorithm will be discussed.

The estimation of a variable $x(t)$ and of its first m derivatives from noisy measurements $y(t)$,

$$y(t) = x(t) + v(t) \tag{12}$$

where $v(t)$ is a Gaussian white noise with variance equal to σ_v^2, can be achieved by building an $(m+1)$-dimensional linear dynamic system

$$\dot{\boldsymbol{x}}(t) = \boldsymbol{A}\boldsymbol{x}(t) + \boldsymbol{B}w(t) \tag{13}$$

where $\boldsymbol{x} = (x, \mathrm{d}x/\mathrm{d}t, \mathrm{d}^2x/\mathrm{d}t^2, \ldots, \mathrm{d}^m x/\mathrm{d}t^m)^T$, $\boldsymbol{A}$ is a square matrix with $m+1$ columns, with $a_{i,j} = 1$, for $j = i+1$, $a_{i,j} = 0$, elsewhere, $\boldsymbol{B} = (0, 0, \ldots, 1)^T$, and $w(t)$ is a white noise signal.

The filtered signal and the estimate of its first m derivatives is obtained via discrete Kalman filtering of a sequence of instrument readings sampled with a sampling time equal to T. The evolution of the state vector $\boldsymbol{X}(k)$ sampled at $t = kT$ is described by the following discrete-time dynamic system, obtained from Eq. (13):

$$\boldsymbol{X}(k+1) = \boldsymbol{\Phi}\boldsymbol{X}(k) + \boldsymbol{W}(k+1) \tag{14}$$

where

$$\boldsymbol{\Phi} = \exp(\boldsymbol{A}T) = \begin{pmatrix} 1 & T & \dfrac{T^2}{2} & \cdots & \dfrac{T^m}{m!} \\ 0 & 1 & T & \cdots & \dfrac{T^{m-1}}{(m-1)!} \\ 0 & 0 & 1 & \cdots & \dfrac{T^{m-2}}{(m-2)!} \\ \vdots & \vdots & \vdots & \ddots & \vdots \\ 0 & 0 & 0 & \cdots & 1 \end{pmatrix}$$

and $\boldsymbol{W}(k)$ is a white noise sequence. Fioretti and Jetto demonstrated[13] that the covariance matrix $\boldsymbol{Q}$ is given by

$$\boldsymbol{Q} = \sigma_w \bar{\boldsymbol{Q}}$$

where the elements of $\bar{\boldsymbol{Q}}$ are

$$\bar{q}_{i,j} = \frac{T^{2m+3-i-j}}{(m+1-i)!(m+1-j)![2m+3-i-j]}$$

Because the only measured state component is the signal, the observation equation is simply

$$y(k) = \boldsymbol{C}\boldsymbol{X}(k) + v(k) \tag{15}$$

where $\boldsymbol{C} = (1, 0, 0, \ldots, 0)$ and $v(k)$ is the white observation noise. Kalman filtering is applied to the discrete-time system obtained from Eqs. (14) and (15). In Refs. 13 and 14, a variance matching technique is used for determining the values of σ_v and σ_w. The steady-state Kalman gains depend only on the ratio σ_w/σ_v, and consequently, given a measurement noise variance σ_v, the whole filtering process is determined by a single scalar quantity σ_w that appears in the definition of the process noise covariance matrix $\boldsymbol{Q}$. When an offline filtering process is possible, the ratio σ_w/σ_v that minimizes the difference between the theoretical and the actual autocorrelation function of the innovation process

$$r(k) = y(k) - \boldsymbol{C}\boldsymbol{\Phi}\hat{\boldsymbol{X}}(k-1|k-1)$$

can be determined for the complete set of available samples $y(k)$, $k = 1, 2, \ldots, N$, where $\hat{\boldsymbol{X}}(k-1|k-1)$ is the state vector estimate at step $k-1$. In this way, suboptimal estimates of both σ_v and σ_w are determined.[13]

In Ref. 13, it is demonstrated also (even if only empirically) that, for sufficiently high sampling rates (low values of T), the estimated value of the sensor noise variance is very close to the actual one. In this way the value of σ_v can be determined from the sensor characteristics. Unfortunately no such a priori estimate is possible for the process noise variance σ_w^2, or, equivalently, for the ratio σ_w/σ_v. As far as $w(t)$ acts as the forcing term in the process described by Eq. (13) or by its discrete version [Eq. (14)], a poor estimate of its variance σ_w^2 produces a bad signal reconstruction. In particular, a high value of σ_w causes the estimated signal to interpolate the noisy samples, leading to unmeaningful high values of the derivatives, whereas the underestimation of σ_w produces excessive filtering action. However, the dependence of σ_w on the actual signal characteristics cannot be taken into proper consideration, because in the present application the filter parameters must be determined before the actual measurements are available. For the purposes of the present study, the value of σ_w is determined filtering offline the sample signal

$$y(t) = 0.25Y_{\max}[1 - \cos(2\pi t/T_{\text{car}})]^2 + v(t) \tag{16}$$

where the parameters $Y_{\max}$ and T_{car} are typical maximum value and characteristic time of the measured quantities, whereas $v(t)$ is a

white noise signal with the same variance as the corresponding sensor noise. The Kalman smoother derived for the sample signal is then implemented in the F-16 fighter aircraft simulation model of Ref. 17 (briefly presented in the next section) to estimate the values of aircraft angular rate and c.g. acceleration components. Note that, when the actual signal is almost constant, all of the true derivatives are close to zero and the estimate of the process noise variance σ_w^2 obtained for the sample signal is clearly exaggerated. Nevertheless, this is not a critical issue, if compared to the drawbacks of an excessive filtering due to a Kalman filter developed for almost constant reference signals, which would seriously degrade the accuracy of computed intrinsic coordinates during maneuvering flight phases, when fast variations of the measured quantities are to be properly estimated.

Finally, a fixed-lag smoother is proposed in Ref. 13 for improving the estimates of the signal and of its derivatives, producing at step k a refined estimate of the signal at step $k-L$, where L is the smoother lag. The smoother is obtained by augmenting the state vector of the system given by Eqs. (14) and (15) with the state variables of the previous L steps, so that the augmented state vector is

$$\boldsymbol{X}^*(k)^T = (\boldsymbol{X}(k)^T, \boldsymbol{X}(k-1)^T, \ldots, \boldsymbol{X}(k-L)^T)$$

whereas the augmented state matrix is

$$\boldsymbol{\Phi}^* = \begin{pmatrix} \boldsymbol{\Phi} & 0 & \cdots & 0 & 0 \\ \boldsymbol{I} & 0 & \cdots & 0 & 0 \\ 0 & \boldsymbol{I} & \cdots & 0 & 0 \\ \vdots & \vdots & \ddots & \vdots & \vdots \\ 0 & 0 & \cdots & \boldsymbol{I} & 0 \end{pmatrix}$$

The observation matrix $\boldsymbol{C}^*$ is obtained adding $(m+1)L$ zeros to $\boldsymbol{C}$, and the process noise covariance matrix is given by

$$\boldsymbol{Q}^* = \begin{pmatrix} \boldsymbol{Q} & 0 & \cdots & 0 & 0 \\ 0 & 0 & \cdots & 0 & 0 \\ 0 & 0 & \cdots & 0 & 0 \\ \vdots & \vdots & \ddots & \vdots & \vdots \\ 0 & 0 & \cdots & 0 & 0 \end{pmatrix}$$

The value of L is determined from the dominant eigenvalue $\lambda_{\max}$ of the nominal Kalman filter dynamic matrix $\boldsymbol{D} = \boldsymbol{\Phi} - \boldsymbol{KC\Phi}$, where $\boldsymbol{K}$ is the steady-state Kalman filter gain matrix, obtained for the nominal system. According to Ref. 13, L should be as high as two or three times the value of $1/\log(\lambda_{\max})$, and as a consequence, it may vary depending on the values of the ratio σ_w/σ_v.

The value of the lag L of the smoother can become as large as 15, for the case of interest in the present application, leading to sizable delays on availability of the smoothed estimates of the signal and its derivatives, with respect to the actual time.

A possible solution for an effective online implementation of the smoother is to sample the signal at a much higher rate than that required by the current application (for example, the refresh rate of the estimated future position on the HUD), so that most of the delay occurs within the refresh time interval and does not affect the pilot perception. If this is not possible, a tradeoff must be found between the best possible smoothing and an acceptable delay that does not degrade the prediction capability of the algorithm. Following the second approach, the value of L is here set to a value lower than that prescribed in Ref. 13. In particular, L was chosen equal to $1/\log(\lambda_{\max})$.

The problem of a proper balance between smoothness and fast response was discussed in Ref. 18, in a similar framework, although on a different timescale. In Ref. 18, a problem of trajectory prediction from radar readings for air traffic control purposes (collision avoidance and conflict resolution) is dealt with, a problem characterized by lower sampling rates and longer prediction horizons. To improve the filter response, an hybrid estimator was proposed, using a weighted combination of the Kalman estimate and the output of an estimator based on an inverse kinematic model. In the approach discussed here, an inverse model cannot be introduced because it is too computationally intense at the sampling rate required for a HUD display or a ground proximity warning system.

Trajectory Prediction

Figure 1 is a flow chart of the trajectory prediction algorithm. The blocks named "signal smoother and derivative estimator" (SSDE) represent the filtering action, with the numbers between parentheses indicating the order of time derivatives estimated during the process. The values of attitude angles provided by the IMU/GPS are necessary for removing the gravity acceleration component from the accelerometer signals. The components of $\boldsymbol{a}_G$ are determined according to Eqs. (9), whereas $\boldsymbol{A}_G$ is computed from Eq. (10), taking into account Eq. (11). These vectors allow for the evaluation of k_1 and k_2, as indicated by Eqs. (2), to provide the coefficients that appear in Eqs. (5) and (6). The position increment $\Delta\boldsymbol{R}_F$ is projected into the body frame using the rotation matrix $\boldsymbol{L}_{BF}$, the components of which are obtained from the unit vectors of the Frenet frame given in Eqs. (1).

III. Results

In this section, the performance of the trajectory prediction algorithm is discussed. In the first part, the capability of the Kalman filter of simultaneously filtering the signals of accelerometers and rate gyros while providing an estimate of their derivatives is analyzed. Then, the capability of predicting future aircraft positions from the estimate of the trajectory intrinsic variables is demonstrated, and a possible visual display of this information, together with an envelope of feasible future positions, is proposed.

A six-degrees-of-freedom model of the F-16 fighter aircraft is used, featuring nonlinear aerodynamics and an engine model based on a first-order lag dynamics.[17] The model order is, thus, equal to 13.

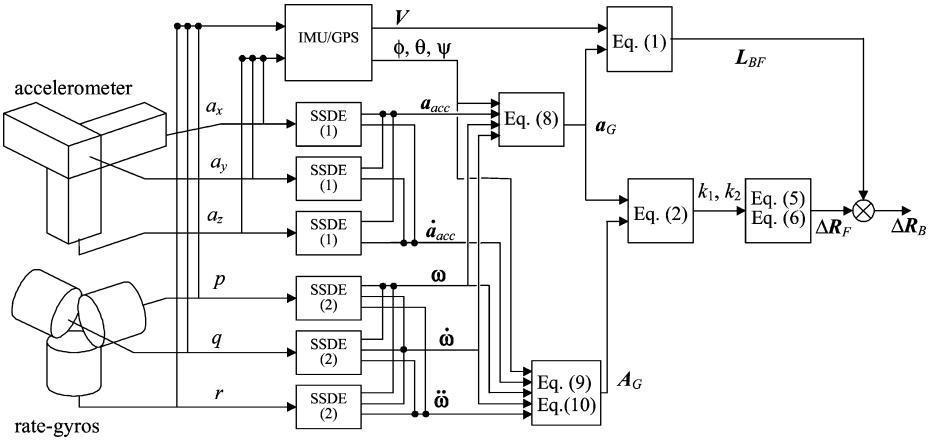

Fig. 1 Flowchart of the trajectory prediction algorithm.

The aircraft c.g. is at 0.30 of the mean aerodynamic chord, to ensure static stability, without the need of modeling the aircraft stability and control augmentation system. The aileron–rudder interconnect (ARI) is modeled, so that the rudder is deflected according to the law

$$\delta_R = K_{\mathrm{ARI}}(\alpha)\delta_A + \delta_{R,\mathrm{pil}}$$

where $\delta_{R,\mathrm{pil}}$ is the pilot command and the ARI gain is given by $K_{\mathrm{ARI}} = 0.13\alpha - 0.7$. In this way, the sideslip angle is kept to below 1 deg in all of the considered maneuvers.

Three turn-reversal maneuvers are performed. Two of them start from a steady turn condition at 400 ft $\cdot$ s^{-1}, with a turn rate of 14.5 deg $\cdot$ s^{-1}. This condition corresponds to maximum turn rate with dry thrust. After 10 s, the ailerons are deflected to reach approximately a symmetric turning condition in the opposite direction in 4.5 (maneuver A) and 9 s (maneuver B), respectively. The roll rate reaches a value of 83 deg $\cdot$ s^{-1} during maneuver A and 35 deg $\cdot$ s^{-1} during maneuver B. In the third maneuver (maneuver C) the initial turn rate is 8 deg $\cdot$ s^{-1}, and the turn reversal is completed in 10 s. The maximum roll rate during maneuver C is 30 deg $\cdot$ s^{-1}. In all cases, the horizontal stabilator deflection and the throttle setting were determined by trial and error to limit as much as possible velocity and altitude variations during the whole maneuver.

Online Implementation of Fixed-Lag Smoother

The number of the derivatives that need to be estimated is actually higher than that strictly required by the trajectory prediction algorithm because the highest order derivative, namely, the mth order, always presents significant amount of noise, even for high values of the smoother lag constant L. However, increasing the order of estimated derivatives produces a Kalman dynamic matrix with eigenvalues closer to the unit circle, that is, with a longer settling time, which, again, requires a higher value for the lag constant L for smoothing. The values $m = 2$ and $m = 3$ were selected for the signals obtained from accelerometers and rate gyros, respectively, thus, minimizing the increase in terms of system order. The Kalman filter for the gyro signals provided a value $\mathrm{int}[1/\log(\lambda_{\max})] = 12$, larger than that obtained for the accelerometer filter, and it was selected as the lag constant for both smoothers, to provide estimates with the same delay. Although in Ref. 13, a value two or three times larger for L is suggested, the smoothing achieved, not optimal from the point of view of signal reconstruction, will prove to be sufficient for the proposed trajectory prediction purposes, as will be shown in the next section.

Using a sampling frequency of 200 Hz, which gives $T = 5$ ms, the trajectory parameters are evaluated with a delay equal to $LT = 60$ ms, a value that appears suitable for possible real-time applications of the prediction algorithm. Note that a delay between 0.12 and 0.18 s results when L is computed as in Ref. 13. The update rate of the estimate will be determined by the lowest frequency in the sensor suite that the algorithm relies on. It is reasonable to assume that this is the IMU/GPS system. For an HUD, the refresh rate should be higher than 0.1 s, to provide a smooth transition between the frames. If the delay LT is kept under the limit of the frame refresh rate, the estimate of the trajectory intrinsic variables is available before the following frame is displayed to the pilot.

Because long intervals with nearly constant values of the measured quantities can be expected during flight, the value of σ_w could drop to very low values. However, a low value of σ_w/σ_v can cause filter divergence, together with an increase in the lag required for the smoother. As a consequence, the Kalman filter gains, determined using the sample signal of Eq. (16), are kept constant throughout the simulated maneuver, regardless of the variation of the sensed variables.

Figures 2a and 2b show the accelerometer signals during maneuver A (thin dotted lines) obtained adding a white noise with variance $\sigma_v = 0.01\ g = 0.32$ ft $\cdot$ s^{-2} to the nominal value of $\boldsymbol{a}_{\mathrm{acc}} = \boldsymbol{a}_A - \boldsymbol{L}_{BI}\boldsymbol{g}$,

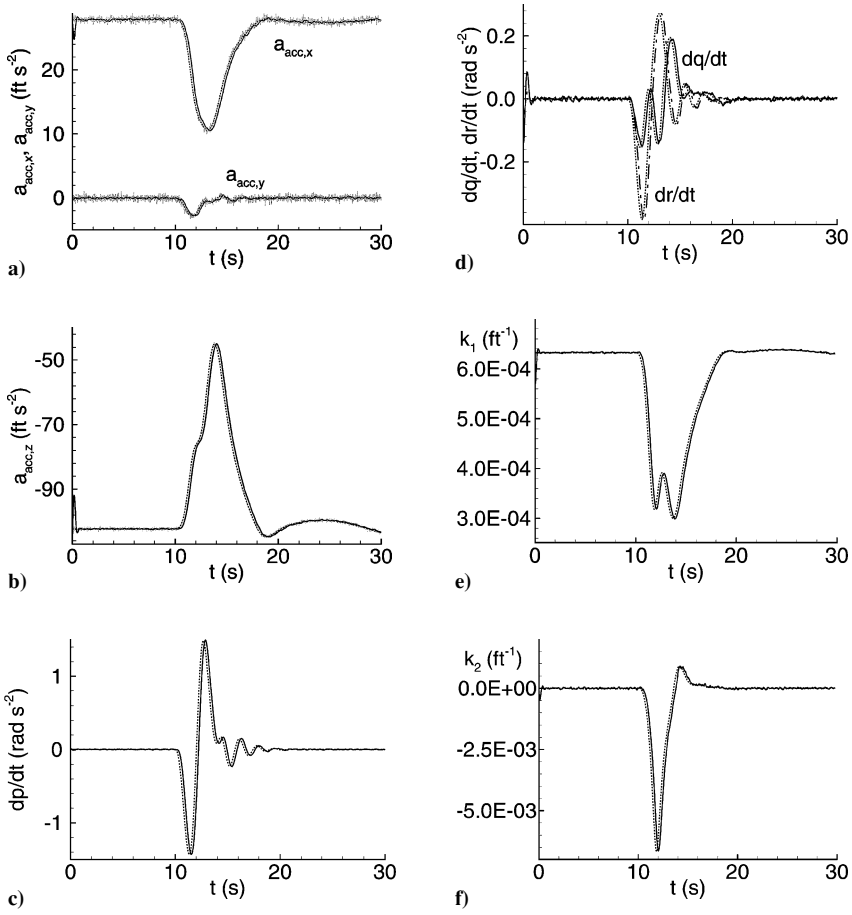

Fig. 2 Estimation for maneuver A: a) and b) accelerometer signals, c) and d) angular velocity derivatives, and e) and f) curvature and torsion.

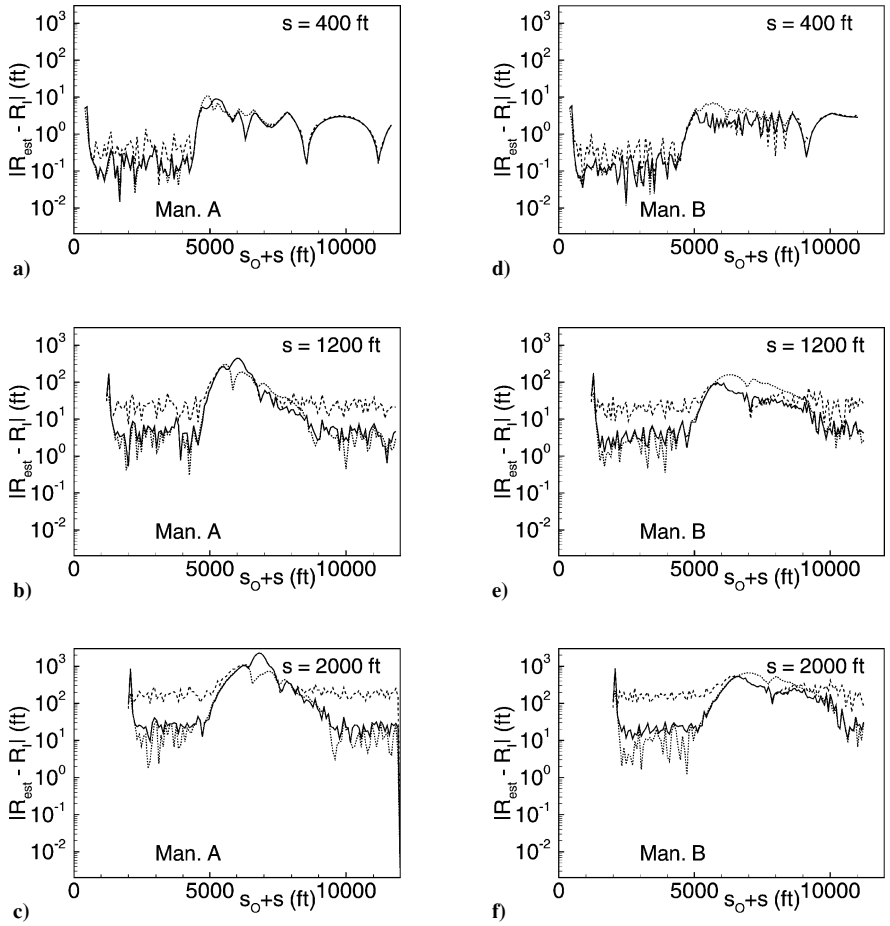

Fig. 3 Error in estimated future position for maneuver A (panels a, b, and c) and maneuver B (panels d, e, and f): ····, Eq. (5); - - - -, Eq. (6); and ——, weighted combination.

determined during the simulation (thick dotted line). The accelerometer position is 10 ft ahead of the aircraft c.g., in the symmetry plane, near the pilot seat. The solid lines represent the filtered value of the signal, which demonstrates a satisfactory filter performance, because the rms of the difference between the actual value and the reconstructed signal is equal to 0.003 g, well below σ_v.

As for the filtering action on the rate-gyro signals, Figs. 2c and 2d show the estimated values of the components of the angular acceleration. In this case, the white noise variance is $\sigma_v = 0.1$ deg $\cdot$ s^{-1}, and also in this case, the error rms for the estimated signal is less then $\frac{1}{3}\sigma_v$. Finally, the estimates of curvature and torsion are reported in Figs. 2e and 2f. These values are fairly close to those determined from aircraft acceleration during the simulation.

In Figs. 2a–2f, the delay in the availability of the estimate with respect to the actual values is clearly visible. Also the effect of the smoother start-up can be observed, in particular in Figs. 2b and 2d, when refined estimates of the variables are not available from the past and a settling time equal to about $3LT$ is necessary for the smoother to converge on a correct (although delayed) estimate.

Trajectory Prediction Algorithm

The prediction error for different increments of the curvilinear abscissa is shown in Fig. 3, for maneuver A (Figs. 3a–3c) and maneuver B (Figs. 3d–3f).

The errors for three different predictions are considered: $\boldsymbol{R}_1(s_0+s)$ (dotted line), determined from Eq. (5); $\boldsymbol{R}_2(s_0+s)$ (dashed line), obtained from the series expansion of Eq. (6); and, finally, a weighted combination $\boldsymbol{R}(s_0+s)$ of the two estimates (solid line),

$$\boldsymbol{R}(s_0+s) = K_W \boldsymbol{R}_1(s_0+s) + (1-K_W)\boldsymbol{R}_2(s_0+s)$$

where the weight is $K_W = 1$, when $\|\dot{\boldsymbol{a}}_G\| < 3$ ft $\cdot$ s^{-3}; $K_W = (20 - \|\dot{\boldsymbol{a}}_G\|)/17$, when $3 \le \|\dot{\boldsymbol{a}}_G\| \le 20$ ft $\cdot$ s^{-3}; and $K_W = 0$ otherwise.

For both basic estimates, $\boldsymbol{R}_1(s_0+s)$ and $\boldsymbol{R}_2(s_0+s)$, the knowledge of the intrinsic variables, and of $\partial k_1/\partial s = V(\partial k_1/\partial t)$, in the case of Eq. (6), at the present time t_0 is sufficient for the position forecast at $t > t_0$. During the steady phases of maneuvers A and B, when both k_1 and k_2 are actually constant, $\boldsymbol{R}_1(s_0+s)$ demonstrates a very high accuracy, in spite of the fact that the statistical properties of the dynamic model of the signal are derived offline for a somewhat arbitrary time-varying reference signal. The prediction error ranges from 0.05% of s, for $s = 400$ ft (Figs. 3a and 3d), to 1%, for $s = 2000$ ft (Figs. 3c and 3f), during the steady ($s_0 < 4500$ ft) and quasi-steady ($s_0 > 9000$ ft) phases.

During the maneuvering phase ($4500 < s_0 < 9000$ ft), the error obtained from a prediction based on the hypothesis of steady state becomes higher than 1%, for $s > 400$ ft. During this segment, the short-term prediction offers a better estimate, in a reduced prediction horizon. The weight K_W was determined to obtain the best combination of the two estimates as a function of the modulus of the derivative of the (estimated) acceleration. Nonetheless, the accuracy of the prediction becomes questionable for increments greater than 800 ft (Figs. 3b, 3c, 3e, and 3f) when the errors becomes as high as 10% of s. However, this can be easily explained when one considers that a prediction based on the current maneuver state cannot be able to anticipate a fast maneuver completed in a time (4 s) of the same order of magnitude of the prediction interval. When less aggressive maneuvers are considered, such as maneuvers C (not shown in the figures), both the predictions $\boldsymbol{R}_1(s_0+s)$ and $\boldsymbol{R}_2(s_0+s)$ become more reliable, even for longer prediction intervals, where the weighted combination is almost coincident with the best one.

Figure 4 shows the results of the trajectory prediction algorithm for maneuver C, at $t_0 = 6$, 12, 15, and 20 s. The gray lines represent the actual trajectory, and the thick ones represent the predicted trajectory. Two cones of feasible positions are also indicated, for each

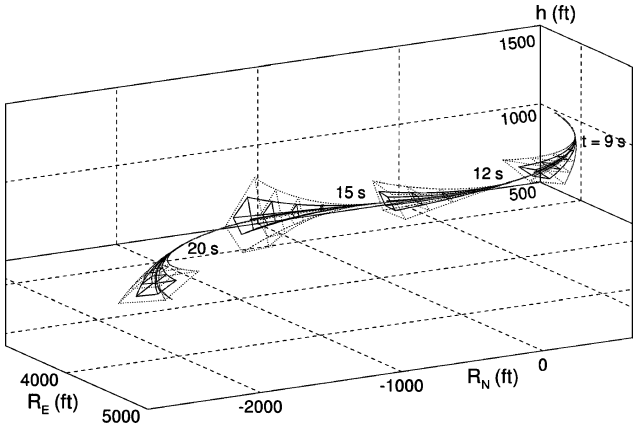

Fig. 4 Trajectory prediction during maneuver C, with representation of cones of feasible future positions.

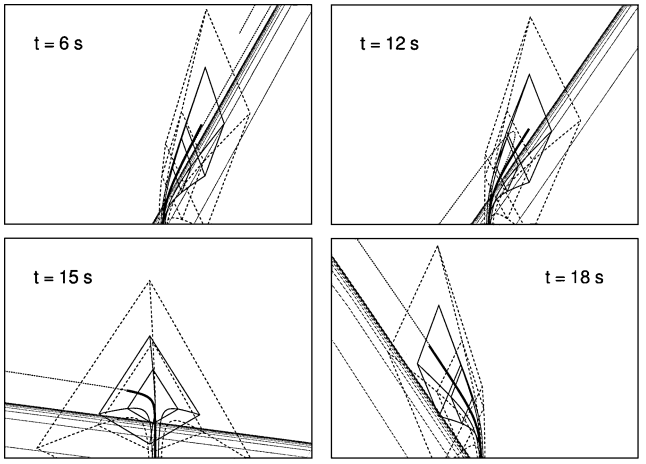

Fig. 5 Perspective display of predicted trajectory and cones of feasible future positions during maneuver C.

initial point. These envelopes are obtained for increments Δn_Z of the normal load factor n_Z and increment $\Delta\phi$ of the roll angle with respect to the current value. The increment $\Delta\phi$ is determined to produce a steady-state increment equal to Δn_Z in a balanced turn. When it is remembered that in this case $\cos\phi = (1/n_Z)$, $\Delta\phi$ satisfies the relation

$$\cos(\phi + \Delta\phi) = 1/(n_Z + \Delta n_Z) \tag{17}$$

where the inner cone is obtained for $\Delta n_Z = 1$, whereas the external one is determined for $\Delta n_Z = 2$.

The maximum load factor constraint can be considered in this phase, limiting the prescribed increments Δn_Z to satisfy the inequality

$$n_Z + \Delta n_Z \leq n_{\max}$$

The edges of the cones are traced neglecting the third-order terms of Eq. (2), in so far as step increments of the perturbed variables n_Z and ϕ are assumed, so that the components of the acceleration vector are not continuous for $t = t_0$.

The cone at $t = 15$ s originates from a position close to the trajectory inflection point, when the wings are almost level. The cone is bended upward, and this means that the pilot would reduce the load factor (negative increment of n_Z) to keep the altitude constant.

The pilot's perspective is also considered in this latter case, and Fig. 5 shows four frames of a perspective view of the actual trajectory (thin line), of the predicted trajectory (thick line) and the envelopes of feasible future positions. The thin straight lines represent the ground and the position of the horizon relative to the cockpit. The pilot's line of sight is assumed to be in a direction parallel to the longitudinal body axis, x_B.

For $t = 6$ s, the aircraft is in a steady turn condition. At $t = 12$ s, it has just entered the maneuvering phase. Of course, the predicted trajectory is tangent to the actual one, but diverges, unaware of the future control inputs from the pilot. Nonetheless, the cone of feasible maneuvers indicates that a roll maneuver with a reduction of the normal load factor is required to perform the desired turn reversal. As stated before, at $t = 15$ s the aircraft is close to the trajectory inflection point. Note how the third-order terms of Eq. (6) allow for a good prediction of the future location even when the curvature is close to zero. In this case, the power series expansion truncated at the second-order terms or a circular flightpath approximation[1–3] would produce a straight line. For $t = 18$ s, the reversal is almost completed, and the picture is practically symmetric with respect to the frame taken at 6 s.

As a final observation, this kind of representation can be used in an HUD during a tracking task, together with the prescribed trajectory or target, to provide the pilot with the information about actual and future positions. The effect of roll and pitch commands is displayed to the pilot by the cones of feasible positions.

IV. Conclusions

An efficient trajectory prediction algorithm is proposed and discussed that solves some of the problems with predictors based on the circular flight-path continuation technique. In particular, the present method demonstrates the possibility to cope with three-dimensional flight-paths, the future positions of the aircraft c.g. being determined on the basis of an algebraic expansion of the trajectory in the Frenet frame. A further advantage of the proposed approach is that the aircraft model is not required because the coefficients of the expansion depend only on kinematic variables and their derivatives. Accelerometer and rate-gyro signal differentiation is accomplished by a Kalman filtering technique, where the process noise is the $m + 1$ derivative of the considered signal. In this respect, an existing algorithm, derived for offline applications, was adapted for the present online implementation. Provided that the coefficient σ_w in the process noise covariance matrix $\boldsymbol{Q}$ is properly determined as a function of the sensor noise covariance σ_v^2, a good estimate of the sensed variables and their derivatives is obtained. Although a signal noise abatement of 70% may not appear a state-of-the-art result in signal processing, it must be remembered that estimate of time derivatives is extremely difficult when dealing with sampled noisy signals.

The trajectory prediction algorithm is evaluated through the simulation of three turn-reversal maneuvers of an F-16 fighter aircraft model. During flight phases characterized by only minor and/or slow variation of aircraft velocity and turn rate, the prediction horizon can be extended almost at will, whereas it is reduced when a very fast variation of the flight condition is commanded, although the short-term behavior is always correctly determined, within a time increment of about 1 or 2 s.

Possible applications of the proposed prediction algorithm in the framework of virtual three-dimensional displays appear promising. As an example, the use of this methodology for heavier transport aircraft with slower response is straightforward and can provide fairly long prediction horizons, suitable for precise flight-path tracking tasks, such as in landing approach. As a first application, envelopes of feasible future positions for increments of normal load factor and roll angle, which correspond to pilot control action about the pitch and roll axes, were considered as a possible visual aid to the pilot. In this latter case, the pilot's perspective was also analyzed, projecting the position vector increment in the body frame, thus producing a perspective view of both the predicted trajectory and the cones of feasible positions.

References

[1]Grunwald, A. J., "Improved Tunnel Display for Curved Trajectory Following: Control Considerations," *Journal of Guidance, Control and Dynamics*, Vol. 19, No. 2, 1996, pp. 370–377.

[2]Grunwald, A. J., "Improved Tunnel Display for Curved Trajectory Following: Experimental Evaluation," *Journal of Guidance, Control and Dynamics*, Vol. 19, No. 2, 1996, pp. 378–384.
[3]Sachs, G., "Longitudinal Flightpath Predictor Design for Minimum Pilot Compensation," *Journal of Aerospace Engineering*, Proceedings Pt. G, Vol. 214, No. G1, 2000, pp. 41–53.
[4]Cheng, V. H. L., and Sridhar, "Considerations for an Automated Nap-of-the-Earth Rotorcraft Flight," *Journal of the American Helicopter Society*, Vol. 36, No. 2, 1991, pp. 61–69.
[5]Clarke, D. W., Mohtadi, C., and Tuffs, P. S., "Generalized Predictive Control—Part I. The Basic Algorithm," *Automatica*, Vol. 23, No. 2, 1987, pp. 137–148.
[6]Clarke, D. W., Mohtadi, C., and Tuffs, P. S., "Generalized Predictive Control—Part II. Extensions and Interpretations," *Automatica*, Vol. 23, No. 2, 1987, pp. 149–160.
[7]Reid, J. G., Chaffin, D. E., and Silverthorn, J. T., "Output Predictive Algorithmic Control: Precision Tracking with Application to Terrain Following," *Journal of Guidance, Control and Dynamics*, Vol. 4, No. 5, 1981, pp. 502–509.
[8]Jung, Y. C., and Hess, R. A., "Precise Flight Path Tracking Using a Predictive Algorithm," *Journal of Guidance, Control and Dynamics*, Vol. 14, No. 5, 1991, pp. 936–942.
[9]Avanzini, G., de Matteis, G., and de Socio, L. M., "Natural Description of Aircraft Motion," *Journal of Guidance, Control and Dynamics*, Vol. 21, No. 2, 1998, pp. 229–233.
[10]Avanzini, G., de Matteis, G., and de Socio, L. M., "Analysis of Aircraft Agility on Maximum Performance Maneuvers," *Journal of Aircraft*, Vol. 35, No. 4, 1998, pp. 529–535.
[11]Miele, A., *Flight Mechanics, Vol. 1, Theory of Flight Paths*, Addison–Wesley, Reading, MA, 1962, pp. 5–9.
[12]Avanzini, G., de Matteis, G., and de Socio, L. M., "Two-Timescale Integration Method for Inverse Simulation," *Journal of Guidance, Control and Dynamics*, Vol. 22, No. 3, 1999, pp. 395–401.
[13]Fioretti, S., and Jetto, L., "Low A Priori Statistical Information Model for Optimal Smoothing and Differentiation of Noisy Signals," *International Journal of Adaptive Control and Signal Processing*, Vol. 8, No. 4, 1994, pp. 305–320.
[14]Hoff, J. C., and Cook, M. V., "Aircraft Parameter Identification Using an Estimation-Before-Modelling Technique," *Aeronautical Journal*, Vol. 100, No. 997, 1996, pp. 259–268.
[15]Kepr, B., "Differential Geometry," *Survey of Applicable Mathematics*, edited by K. Rektorys, MIT Press, Cambridge, MA, 1969, pp. 306–317.
[16]Etkin, B., *Dynamics of Atmospheric Flight*, Wiley, New York, 1972, Chap. 5, pp. 152–154.
[17]Stevens, B. L., and Lewis, F. L., *Aircraft Control and Simulation*, Wiley, New York, 1992, pp. 25–27, 584–592.
[18]Chatterji, G. B., "Short-Term Trajectory Prediction Methods," AIAA Paper 99-4233, Aug. 1999.